The electron momentum density of copper studied by (gamma , e gamma) spectroscopy

1991 J. Phys.: Condens. Matter 3 5587

(http://iopscience.iop.org/0953-8984/3/29/012)

J. Phys.: Condens. Matter 3 (1991) 5587–5601. Printed in the UK

The electron momentum density of copper studied by (γ, eγ) spectroscopy*

F Bell†, Th Tschentscher‡, J R Schneider‡ and A J Rollason§

† Sektion Physik, Universität München, Am Coulombwall 1, 8046 Garching, Federal Republic of Germany

‡ Hamburger Synchrotronstrahlungslabor (HASYLAB), Notkestrasse 85, 2000 Hamburg 52, Federal Republic of Germany

§ Department of Physics, University of Keele, Staffordshire ST5 5BG, UK

Received 8 March 1991

Abstract. We report coincidence measurements between inelastically scattered 148 keV photons and the recoil electrons generated within a 80 nm thin Cu foil. We have analysed the Doppler broadening of the scattered photon intensity, which corresponds to a scan through the three-dimensional electron momentum density (EMD) parallel to the momentum transfer vector. The experimental data are compared with a theoretical EMD from the modified augmented plane wave method. A Monte Carlo calculation is described that allows for the correction of multiple electron scattering within the foil. Estimates of the triple-differential cross section for Compton scattering are given. The experiment was performed with the synchrotron radiation from a bending magnet of the DORIS storage ring at Deutsches Elektronen-Synchrotron (DESY), Hamburg, Federal Republic of Germany.

1. Introduction

In the past, inelastic high-energy photon scattering (i.e. Compton scattering) has been used to investigate the so-called Compton profiles of valence electrons from solids. The momentum distribution of the initially bound electrons causes a Doppler broadening of the scattered radiation. If the recoil electron is not observed, the double-differential cross section for the scattered photon is proportional to an integration of the momentum density over the momentum components, which are perpendicular to the photon momentum transfer vector $\boldsymbol{K} = \boldsymbol{k} - \boldsymbol{k}'$. Here, $\boldsymbol{k}$ and $\boldsymbol{k}'$ are the momenta of the primary and scattered photon respectively. However, if the electron is detected in coincidence with the scattered photon, the scattering kinematics are determined completely and the triple-differential cross section becomes proportional to the electron momentum density (EMD) itself. In traditional Compton scattering the EMD can only be obtained by measuring a large number of directional Compton profiles and employing reconstruction techniques (Hansen *et al* 1987).

Recently, we have demonstrated that the EMD of Al can be extracted from such a (γ, eγ) experiment (Rollason *et al* 1989a, b, Bell *et al* 1990). The idea of fixing the kinematics by a coincidence condition is the same as used in positron annihilaton

* Dedicated to Professor Heinz Maier-Leibnitz on the occasion of his 80th birthday.

0953-8984/91/295587 + 15 $03.50

experiments or in (e, 2e) spectroscopy, which means that the results one gains from all three experimental techniques are similar or even identical. In the positron experiment the annihilation rate is proportional to the square of the Fourier transform of the product of the positron and electron wave functions (Berko 1983). Thus, for information about the EMD it may be advantageous to use $(\gamma, e\gamma)$ experiments, since any ambiguity due to the positron wave function is avoided. The similarity between (e, 2e) and $(\gamma, e\gamma)$ spectroscopy is even greater: in both cases the triple-differential cross section is proportional to the EMD, the proportionality factor being, roughly speaking, the Rutherford cross section in the former case and the Klein–Nishina cross section in ours (Byron and Joachain 1989, McCarthy and Weigold 1988, Rollason *et al* 1989b). The strong electron–nucleon interaction in (e, 2e) produces severe incoherent elastic multiple scattering within solid-state foils. This smearing of the electron direction disturbs, to some extent, the evaluation of the EMD. Although this effect also exists in our case, it is less important than for (e, 2e) spectroscopy since one of the collision partners is a photon, restricting the multiple-scattering effect to the recoil electron only. This is probably why there have been so few attempts to apply (e, 2e) spectroscopy to solids (Persiantseva *et al* 1979, Ritter *et al* 1984, Gao *et al* 1988, Hayes *et al* 1988, 1991).

Finally, we should mention some early $(\gamma, e\gamma)$ experiments dating back to the beginning of quantum mechanics. It should be remembered that the coincidence method was invented in 1925 by Bothe and Geiger (1925) while studying the Compton effect. Experiments after this increased both the time and angular resolution (Bothe and Maier-Leibnitz 1936, Cross and Ramsey 1950) but only the more recent experiments (Rollason *et al* 1989a, b, Bell *et al* 1990) were able to show the influence of the intrinsic EMD of the bound electron. These experiments have become possible with access to the new powerful sources of γ-rays represented by modern lepton storage rings. In the following we describe such an experiment at the storage ring DORIS II at Deutsches Elektronensynchrotron (DESY), Hamburg, which yielded the momentum density of copper.

2. Kinematics

In this section we discuss the kinematical situation of $(\gamma, e\gamma)$ experiments. If a photon with initial energy ω and momentum k is inelastically scattered by an electron at rest (using natural units, i.e. $m = \hbar = c = 1$ and $e^2 = \alpha$, the fine structure constant) a photon detector, placed at an angle θ_0, will measure a photon with energy ω_0'

$$\omega_0' = \omega/[1 + \omega(1 - \cos\theta_0)]. \tag{1}$$

Simultaneously, the recoiling electron will be emitted at an angle φ_0 with respect to the primary photon direction

$$\cot\varphi_0 = (1 + \omega)\tan(\theta_0/2) \tag{2}$$

and with an energy

$$E_0' = \omega - \omega_0' + 1 \tag{3}$$

(remember that E_0' is the total energy including the rest mass energy). Now, let the electron be bound with a binding energy $E_B > 0$ and an EMD $\rho(p)$. From the momentum

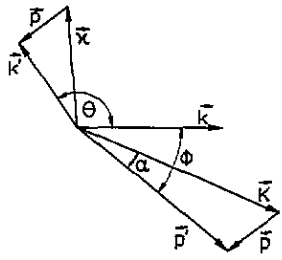

Figure 1. Momentum diagram of the scattering process.

diagram of figure 1 it follows that the result is two fold: electrons will appear at angles $\varphi \neq \varphi_0$ and the photons will have energies $\omega' \neq \omega_0'$. The following quantitative analysis refers to our experimental set-up, where the photon detector was fixed at an angle $\theta = \theta_0$ and the electron detector could be placed at arbitrary angles φ. In this case the energy broadening $\Delta\omega' = \omega' - \omega_0'$ is, in essence, given by the initial momentum component p_z of the electron parallel to momentum transfer vector $\boldsymbol{K}$, and the angular broadening $\Delta\varphi = \varphi - \varphi_0$ by the components $p_\perp$ perpendicular to $\boldsymbol{K}$. Since $\boldsymbol{p} = \boldsymbol{k}' - \boldsymbol{k} + \boldsymbol{p}'$, it can be seen from figure 1 that

$$p_z = p' \cos\alpha - K \tag{4a}$$

$$p_\perp = p' \sin\alpha \tag{4b}$$

where the final electron momentum $\boldsymbol{p}'$ is given by

$$p' = [(\omega - \omega' + 1 - E_B)^2 - 1]^{1/2} \tag{5}$$

and the transfer vector K is given by

$$K = (\omega^2 + \omega'^2 - 2\omega\omega' \cos\theta_0)^{1/2} \tag{6}$$

where the angle α between $\boldsymbol{K}$ and $\boldsymbol{p}'$ is given by

$$K \cos\alpha = \omega \cos\varphi - \omega' \cos(\varphi + \theta_0). \tag{7}$$

The last equation holds for a coplanar detector arrangement only. Whereas equations (4) are exact, we shall derive approximate expressions that show the connection between the initial momentum components $(p_\perp, p_z)$ and either the Doppler broadening $\Delta\omega'$ or the angular correlation $\Delta\varphi$. For high-energy photons it is well known that the momentum transfer vector $\boldsymbol{K}$ does not vary significantly in either length or direction over the range of scattered photon energies ω' that are of interest. Therefore, we use the approximation

$$K \simeq K_0 = (\omega^2 + \omega_0'^2 - 2\omega\omega_0' \cos\theta_0)^{1/2}. \tag{8}$$

The maximum value of the angle α is roughly given by $\sin\alpha \simeq p_F/K_0$ where the Fermi momentum p_F is about 1 au and $K_0 \simeq 60$ au for our experimental situation. Thus, $\alpha \ll 1$ and we obtain (4)

$$p_z = p' - K \simeq (\omega/K_0\omega_0')\,\Delta\omega' \tag{9a}$$

$$p_\perp \simeq p'\alpha \simeq K_0\,\Delta\varphi. \tag{9b}$$

In (9*a*) additional terms of the order E_B/K_0 have been neglected. We will discuss this in section 5. In principle, the $(\gamma, e\gamma)$ experiment can be run in two ways: either both

detectors are fixed, i.e. the electron detector is also placed at $\Delta\varphi$ = constant—in this case one obtains a p_z-scan through the EMD $\rho(\boldsymbol{p})$ for a fixed $p_\perp$ by measuring the Doppler broadening $\Delta\omega'$ in the γ-detector–or the angular correlation is measured by scanning the electron detector over a range of $\Delta\varphi$-values. Then a $p_\perp$-scan for a fixed p_z-value is made if coincidences at constant ω'-values are detected in the γ-detector. We have tested both possibilities (Rollason *et al* 1989b, Bell *et al* 1990). Since no position-sensitive detector was available we had to move the electron detector and to count coincidences at each angle. Therefore, the angular correlation method is more time consuming by far (for a fixed statistical error of the coincidence counts) than the Doppler broadening technique. For this reason we restricted the present experimental data to p_z-scans.

Finally, we emphasize that the analysis above referes to a fixed photon detector at $\theta = \theta_0$. Of course, one could do the same for a fixed electron detector at $\varphi = \varphi_0$ and move the photon detector. We will give the approximate expressions only: the initial electron momentum $\boldsymbol{p}$ can be decomposed into components parallel and perpendicular to the vector $\boldsymbol{\kappa}_0 = \boldsymbol{k} - \boldsymbol{p}_0'$. The component p_z parallel to $\boldsymbol{\kappa}_0$ yields a Doppler broadening $\Delta E' = E' - E_0'$ in the electron detector:

$$p_z = \omega' - \kappa_0 \simeq [(1+\omega)/(1+E_0')\kappa_0]\,\Delta E' \tag{10a}$$

and the component $p_\perp$ perpendicular to $\boldsymbol{\kappa}_0$ yields an angular correlation

$$p_\perp = \kappa_0\,\Delta\theta \qquad \Delta\theta = \theta - \theta_0 \tag{10b}$$

where

$$E_0' = (1+x^2)/(1-x^2) \qquad x = \omega\cos\varphi_0/(1+\omega)$$

and

$$\kappa_0 = (\omega^2 + p_0'^2 - 2\omega p_0' \cos\varphi_0)^{1/2} \tag{11}$$

with

$$p_0' = (E_0'^2 - 1)^{1/2}.$$

In analogy to two-dimensional angular correlation of annihilation radiation—2D ACAR (Berko 1983)—in an ideal $(\gamma, e\gamma)$-experiment two two-dimensional photon and electron detectors could be placed with their centres at θ_0 and φ_0. Depending on their energy resolution the p_z-components of the EMD could be resolved or not. In contrast to the case for 2D ACAR, the approximations (9) and (10) for both detectors do not hold equally well. Whereas (9) is a very good approximation for $K \gg p$, equation (10) is valid only if $\boldsymbol{\kappa}_0$ points in strong backward directions, i.e. if $\theta \simeq \pi$ holds. This demonstrates the asymmetric behaviour of the γ-ray and electron branches.

3. Experiment

The experiment was performed using the synchrotron radiation from a bending magnet of DORIS II at DESY with a critical energy of $E_c = 27$ keV. The beam was monochromated with a single Ge crystal in (220) transmission. The energy width of the primary photon beam, originating from the beam divergence and the rocking curve width of the Ge crystal, was about 1 keV at $\omega = 148$ keV. The γ-ray entered an evacuated target chamber of 0.8 m diameter with an externally mounted intrinsic Ge detector at a scattering

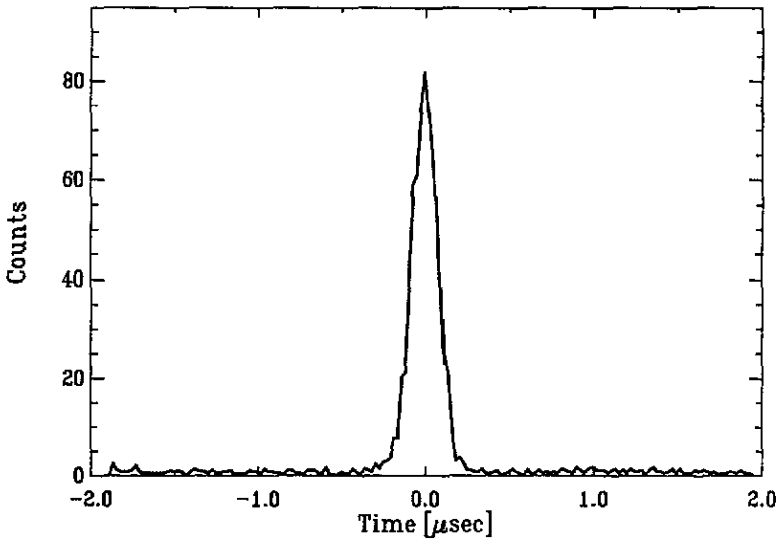

Figure 2. Time spectrum for a 0.5 μm thin Al foil.

angle $\theta_0 = 140°$ and a passivated implanted planar silicon diode as an electron detector mounted internally at an angle $\varphi = \varphi_0 = 15.8°$. It has been shown that the momentum resolution of a Compton scattering spectrometer operating with a solid-state detector at a scattering angle of 140° is best for photon energies around 150 keV (Manninen *et al* 1990). The incident beam and both detectors were coplanar. The energy resolution of the electron detector (= 10 keV FWHM) was poor compared to that of the Ge diode (= 0.8 keV). The latter, together with the energy width of the primary beam, yielded an energy uncertainty which, in turn, can be transformed via (9*a*) to a p_z-resolution of the experiment with $|\Delta p_z| = 0.9$ au (FWHM). At the same time both the angular acceptance of the photon and the electron detector introduced via (9*b*) a momentum uncertainty $|\Delta p_\perp| = 0.6$ au.

The storage ring was operated in the single-bunch mode with a bunch distance τ_B = 960 ns and a bunch length of 0.15 ns which is small compared with the time resolution τ of our coincidence circuit (160 ns FWHM). Under these conditions the accidental coincidence count rate $\dot{n}_a$ is determined by uncorrelated events within the same bunch. Thus, $\dot{n}_a$ is independent of τ and is given by $\dot{n}_a = \dot{n}_1 \dot{n}_2 \tau_B$, where $\dot{n}_1$ and $\dot{n}_2$ are the photon- and electron- detector count rates. (To be more specific, the $\dot{n}$ are the macroscopic count rates averaged over a long time; they are not the count rates during a bunch.) Since τ_B is very large and the bunch length is much shorter than the time resolution of modern slow–fast coincidence circuits the experiment must inevitably be performed with extremely low single-count rates $\dot{n}_1$ and $\dot{n}_2$. We used very thin self-supporting Cu foils (80 nm), thus keeping the accidental count rate at an acceptable level.

Figures 2 and 3 show the time spectra for 0.5 μm (figure 2) and 50 μm (figure 3) thin Al foils which were taken under otherwise identical conditions. If we disregard for a moment the effect of electron multiple scattering within the foil, we expect that the ratio of true to accidental events decreases proportionally to $1/d$ where d is the foil thickness. Multiple scattering, which tends to limit the count rate in the electron detector, will weaken this dependence but the trend will remain and is clearly seen by comparison of

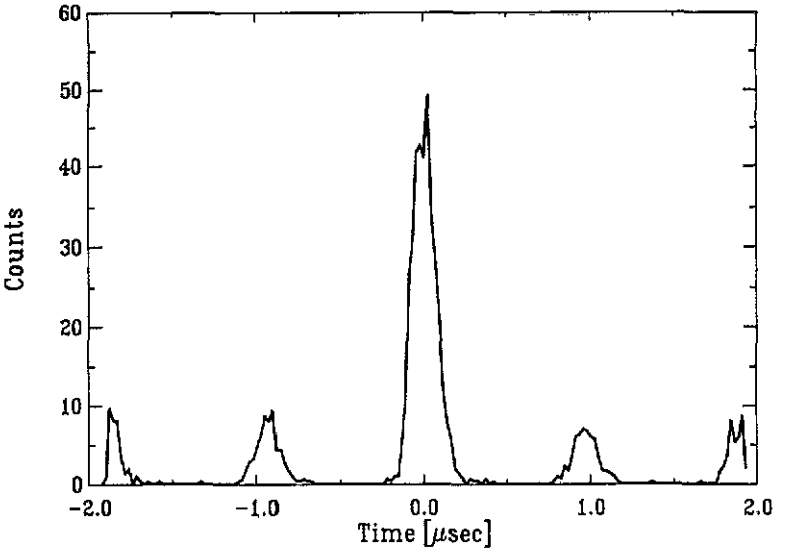

Figure 3. Time spectrum for a 50 μm thin Al foil.

the figures. Whereas the 0.5 μm foil shows practically no accidental events, satellites due to uncorrelated events from neighbouring bunches appear for the 50 μm foil. The time spectrum for the 80 nm Cu foil is identical with that of figure 2.

3.1. Monte Carlo correction

As mentioned in the introduction, an essential point of the experiment is the multiple scattering of the recoil electrons within the target foil. In the following we will describe a Monte Carlo (MC) procedure with which we have corrected our experimental data for this effect. Since, for our experimental set-up, the average kinetic recoil energy is $E_0' = 50$ keV ($\omega_0' = 98$ keV), the mean free path λ for elastic scattering is about 12 nm in Cu. Since the electrons are homogeneously produced throughout the 80 nm foil they experience on average about three collisions. Although this is a rather large number of collisions the experiment is redeemed by the fact that the differential electron scattering cross section is strongly peaked in the forward direction, which is in marked contrast to inelastic photon scattering. In order to retain maximum flexibility, we decided not to simulate the whole experiment by a Monte Carlo (MC) calculation but only the transmission of those electrons that had started within the foil in a direction parallel to the momentum transfer vector $\boldsymbol{K}_0$. If one knows the distribution $g(\boldsymbol{p}_\perp)$ in the transverse momenta $\boldsymbol{p}_\perp$, which are the momenta the electrons have after leaving the foil, the measured electron intensity is a convolution of $g(\boldsymbol{p}_\perp)$ with the undisturbed emission pattern. Since the latter is proportional to the three-dimensional EMD $\rho(\boldsymbol{p})$, the measured electron intensity I becomes

$$I(\boldsymbol{p}_\perp, p_z) = A\left(P_0\rho(\boldsymbol{p}_\perp, p_z) + (1 - P_0)\int \rho(\boldsymbol{p}_\perp' - \boldsymbol{p}_\perp, p_z)g(\boldsymbol{p}_\perp')\,\mathrm{d}^2\boldsymbol{p}_\perp'\right) \tag{12}$$

where A is a constant (which includes the cross-section, solid angles etc) and P_0 is the fraction of unscattered electrons:

$$P_0 = (\lambda/d)(1 - e^{-d/\lambda}) \tag{13}$$

where d is the foil thickness (see remarks below), and the distribution function $g(\boldsymbol{p}_\perp)$ is

normalized to unity. As a first-order correction we take the ratio $R(p_\perp, p_z)$ of the undisturbed electron intensity to that of the intensity influenced by multiple scattering

$$R(p_\perp, p_z) = A\rho(p_\perp, p_z)/\langle I(p_\perp, p_z)\rangle_{av} \tag{14}$$

by which the experimental data should be multiplied in order to obtain corrected data. Here, $\langle \ldots \rangle_{av}$ means that we have averaged the scattered intensity I over the finite opening of the electron detector and convoluted with the energy resolution of the γ-detector. For our model we have evaluated the correction factor for $p_\perp = 0$.

In the following we describe briefly the MC procedure to obtain the distribution function $g(p_\perp)$. The method is very similar to that used by Felsteiner *et al* (1974) for the multiple-scattering correction of inelastically scattered photons. But, in contrast to MC programs for photons, our simulation is very much facilitated by the simple geometry of our targets, thus allowing a calculation in cylindrical coordinates. At 50 keV the first Born approximation works very well and the Mott–Born cross section is (Motz *et al* 1964, Salvat 1991)

$$d\sigma/d(q^2) = \pi(2Z/v)^2[1 - (q/2\gamma c)^2]f^2(q^2). \tag{15}$$

Equation (15) is written in atomic units. The form factor f for a solid differs from that for a free atom since, in the former case, an atom is completely screened within the Wigner–Seitz radius. Salvat and Parellada (1984b) have given expressions for f that were obtained from Dirac–Slater self-consistent electron densities under the appropriate Wigner–Seitz boundary conditions:

$$f(q^2) = A/(\alpha_1^2 + q^2) + (1 - A)/(\alpha_2^2 + q^2) \tag{16}$$

with $A = 0.213\,74$, $\alpha_1 = 13.4817$ and $\alpha_2 = 2.429\,97$ for Cu. Z is the nuclear charge of the target, v is the electron velocity, $\beta = v/c$, $\gamma^2 = 1/(1 - \beta^2)$ and $c = 137$, the velocity of light. Here, $q = 2p_0' \sin(\alpha/2)$, which is the momentum transfer when electrons with momentum p_0' are scattered by an angle α.

For the MC procedure we have used the method of forced collisions (Cashwell and Everett 1959, Felsteiner *et al* 1974). If the distance to the exit surface is Δ we force the electron to have its next collision after a path length

$$s = -\lambda \ln[1 - r(1 - \exp(-\Delta/\lambda))] \tag{17}$$

where r is a random number with $0 \leq r \leq 1$. To allow for the part of the flux that would otherwise be transmitted without a collision the electron is assigned a weight

$$W = 1 - \exp(-\Delta/\lambda). \tag{18}$$

The mean free path $\lambda = (N\sigma)^{-1}$ is obtained from the total cross section

$$\sigma = \int \frac{d\sigma}{d(q^2)}\, d(q^2)$$

and the number density N of the target atoms. Due to the cylindrical symmetry of the scattering geometry one needs only to follow the z-components z_i of the electron

trajectories. This component is both parallel to K_0 and the surface normal of the foil. One obtains for successive collisions

$$z_{i+1} = z_i + s \cos \gamma_{i+1} \tag{19}$$

where γ_{i+1} is the angle between the trajectory and the z-axis after the ith collision. From geometry one finds

$$\cos \gamma_{i+1} = \cos \gamma_i \cos \alpha - \sin \gamma_i \sin \alpha \cos \beta \tag{20}$$

where α and β are the polar and azimuthal scattering angles at the ith collision. The point within the foil where the electron starts with $\gamma_0 = 0$, the path length s, the azimuthal angle β and the polar scattering angle α were obtained from random numbers. The latter were calculated from the momentum transfer q which was sampled from (15) by using the so-called composition method (Rubinstein 1981, Salvat *et al* 1986).

We have used a version of the MC procedure where each electron experiences a fixed, preselected number i_{max} of collisions. The probability of undergoing i collisions is Poisson distributed which, in our case, means averaged over the foil thickness:

$$P_i(x) = \frac{1}{x}\left(1 - e^{-x} \sum_{\nu=0}^{i} \frac{x^\nu}{\nu!}\right) \tag{21}$$

with $x = d_{eff}/\lambda$. d_{eff} is an effective foil thickness which incorporates the effect of path length increase by lateral scattering. We have checked (21) with our MC calculation and found very good agreement if d_{eff} is identified with the foil thickness d. This demonstrates that, due to the strong forward peaking of the electron differential cross section, lateral scattering is negligible (Kwei 1984). We have chosen $i_{max} = 12$. It is easily verified that for $x = 6.6$, which applies to our experiment, $P_{12} \ll P_0$ holds. (This can also be seen from the first two moments of distribution (21), which determine the average number of collisions within the foil $\langle i \rangle = x/2 = 3.3$ and the variance $\sigma^2 = \langle i^2 \rangle - \langle i \rangle^2 = x/2 + x^2/12 = 6.9$.) After the last collision, electrons were sampled according to their transverse momenta $p_\perp = p_0' \sin \gamma$. This procedure yields the distribution $g(p_\perp)$ of (12).

The basic assumption for the correction procedure is that angular spreading is dominated by incoherent elastic scattering and that the influence of inelastic scattering on angular dispersion can be neglected (Reimer 1984, Salvat and Parellada 1984a, b, Lencinas *et al* 1990). Roughly, the cross section for the elastic electron–nucleus interaction scales with Z^2 whereas the inelastic electron–electron interaction scales only with Z. It is for this reason that some authors replace Z^2 by $Z(Z + 1)$ in (15) (see e.g. Brown *et al* (1969) and further references therein). In addition, we have disregarded the slowing down of the electrons since the average energy loss in our foils amounts to 0.15 keV only (Pages *et al* 1972) which is small compared with the resolution of our γ-detector. The production of secondary or cascade electrons is believed to play no essential role at our electron energies (Salvat *et al* 1986).

5. Experimental results

Figures 4 and 5 show the non-coincident (figure 4) and the coincident photon spectrum of the 80 nm Cu foil (figure 5). The spectrum of figure 4 has been obtained after the subtraction of a 10% flat background. The original ω'-dependence was converted into a p_z-scale using (9*a*). For comparison, the solid line in figure 4 represents the

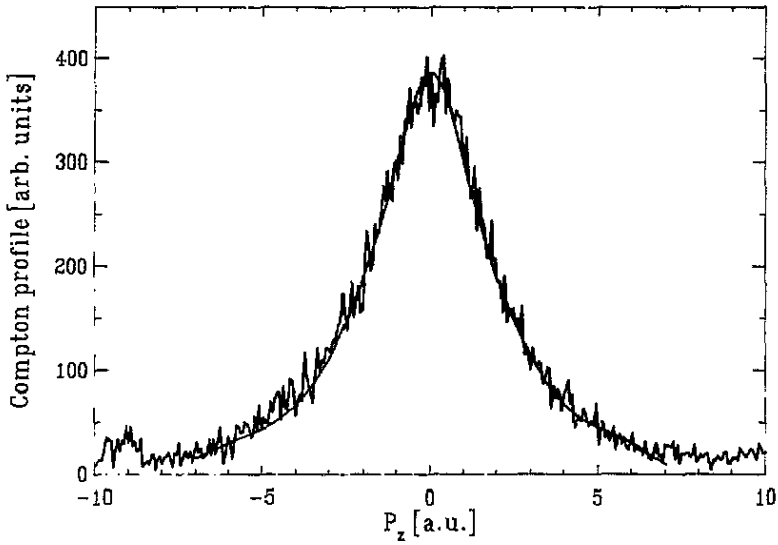

Figure 4. The single-photon counts as a function of p_z. The solid curve represents the data of Paakkari *et al* (1975).

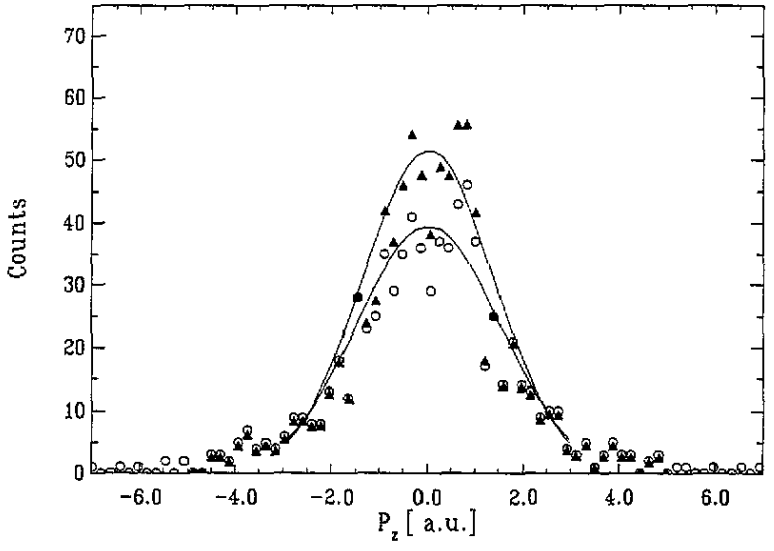

Figure 5. Coincidence counts as a function of p_z. The raw data (circles) have been corrected for multiple scattering (triangles). The curves have been drawn to guide the eye.

experimental data from Paakkari *et al* (1975) which have been folded with our p_z-resolution of 0.9 au (FWHM). We remark that our foil is about a factor 10^4 thinner than targets usually used in conventional Compton scattering work. In figure 5 both the experimental raw data (open circles)—the integrated coincidence count rate was about 7 mHz—and those corrected for multiple scattering (full triangles) are shown. In the

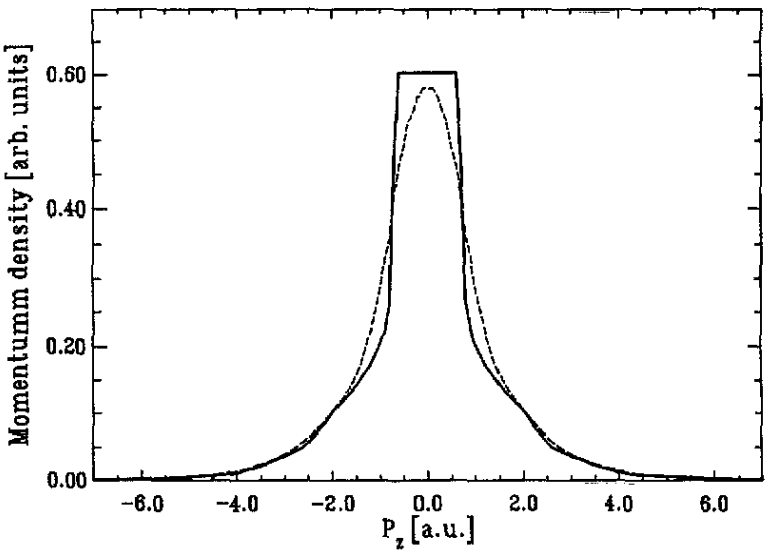

Figure 6. The MAPW momentum density of Bross (1982) (solid curve) and convoluted with the experimental p_z-resolution (broken curve).

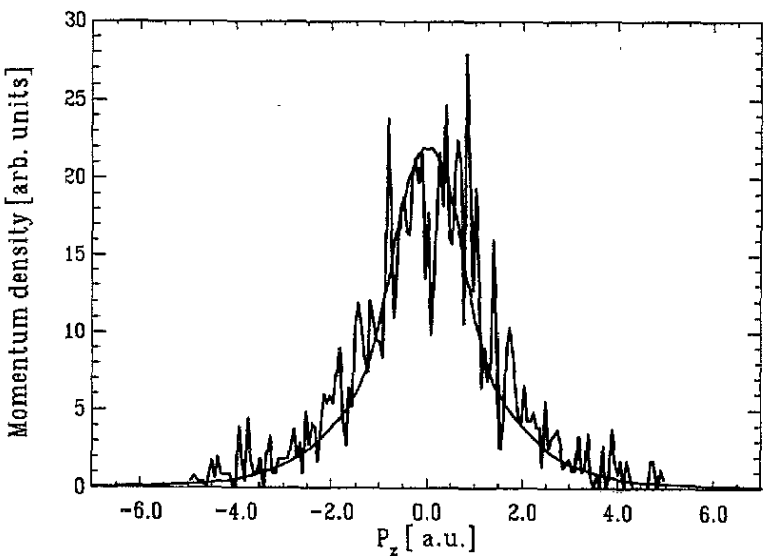

Figure 7. Comparison of the corrected coincidence count rate with the convoluted EMD (solid curve). Both have been normalized at the maximum.

latter case the raw data have been multiplied by the correction factor $R(0, p_z)$ of (14). For the evaluation of R one needs the EMD $\rho(\boldsymbol{p})$. At least two strategies seem to be appropriate. As a first-order approximation one could use the experimental data of figure 5 (the raw data) or, alternatively, one could start with a simple and rather crude theoretical model for $\rho(\boldsymbol{p})$. In view of the rather large statistical fluctuations of the

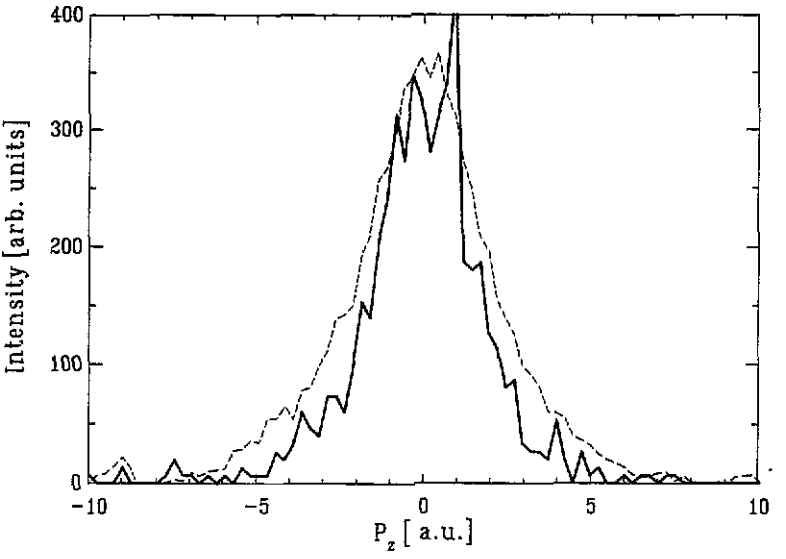

Figure 8. Comparison of the corrected coincidence count rate (solid curve) with the single-photon count rate (broken curve).

experimental data we decided to take the second possibility. For the $(4s)^1$ state in Cu we used a Seitz approximation with Fourier components of the Bloch waves extracted from experimental work (Pattison *et al* 1982). The strongly anisotropic EMD has been spherically averaged like the similar renormalized free-atom model of Berggren (1972). All other states were treated as atomic-like. The wave functions for these states, obtained by a Roothaan–Hartree–Fock method, are tabulated by Clementi and Roetti (1974) in the form of Slater-type orbitals, which can easily be Fourier transformed into momentum space.

Finally, we want to compare our data with an EMD obtained from sophisticated band structure calculations. Bross (1982) has used the modified augmented plane wave method (MAPW) to calculate the spherically averaged EMD in Cu including even the $(3s)^2$ and $(3p)^6$ states into the band structure. Figure 6 shows $\rho(p)$ as a function of $p = p_z$ (since $p_\perp = 0$). The solid curve represents the data of Bross whereas the dotted curve was obtained after a convolution with our p_z-resolution. We have checked that the $(1s)^2$ $(2s)^2$ $(2p)^6$ core makes no contribution to $\rho(p)$ which is visible on the scale of figure 6. Therefore, the deepest core level which has been accounted for in the MAPW density is the 3s state with a binding energy E_B of 122.5 eV (Fuggle and Martensson 1980). We have mentioned that in (9*a*), terms of the order E_B/K_0 ($\simeq 0.073$ au for the 3s state) have been neglected which can now be justified. In figure 7 the convoluted EMD is compared with the corrected data of figure 5. In view of the statistical fluctuations the agreement is acceptable. In figure 8 we compare the coincident photon spectrum with the non-coincident one, normalized to the maximum. It is evident that the former is remarkably narrower. This should be the case, since the Compton profile

$$J(p_z) = \int\int \rho(p_x, p_y, p_z)\, \mathrm{d}p_x\, \mathrm{d}p_y \tag{22}$$

sums over the long-ranging momentum density contributions in the x- and y-directions.

The experimental data of figures 4 and 5 allow a crude test of the triple-differential cross section for inelastic photon scattering from bound electrons. To our knowledge such a test has never been previously performed, although the cross section is one of the most fundamental in atomic physics. For large momentum transfer $K_0 \gg p$ the cross section can be written (Rollason *et al* 1989a) as

$$\frac{d^4\sigma}{d\omega'\, dE'\, d\Omega_\gamma\, d\Omega_e} = \left(\frac{d\sigma}{d\Omega_\gamma}\right)_{KN} \frac{\omega K_0}{\omega_0'} \sum_i \rho_i(p)\delta(\omega - \omega' - E' - E_B^i + 1) \tag{23}$$

where $(\ldots)_{KN}$ is the Klein–Nishina cross section for the scattering of a photon at an electron at rest (Jauch and Rohrlich 1955), and ρ_i and E_B^i are the EMD and separation energy of the single-particle state i. For $K_0 \simeq p_0'$, and also in the non-relativistic limit, the cross section of (23) becomes identical to that given by Platzman and Tzoar (1965). We note that the structure of (23) is the same either for (e, 2e), (γ, eγ) in atomic and solid state physics (Byron and Joachain 1989) or for (e, e'p) and (p, 2p) reactions in nuclear physics (Antonov *et al* 1988, Day 1989). Since from (9*b*) the differential solid angle of the electron detector is

$$d\Omega_e = dp_x\, dp_y / K_0^2 \tag{24}$$

we obtain from (23)—ignoring the binding energies E_B^i and performing the δ-function integration—the well-known double-differential cross section (Cooper 1985)

$$d^2\sigma/d\omega'\, d\Omega_\gamma = (d\sigma/d\Omega_\gamma)_{KN}(\omega/\omega_0' K_0) J(p_z) \tag{25}$$

with p_z from (9*a*). Integration of (23) and (25) over the scattered photon energy ω' yeilds, due to (9*a*),

$$\frac{d^2\sigma}{d\Omega_\gamma\, d\Omega_e} = \left(\frac{d\sigma}{d\Omega_\gamma}\right)_{KN} K_0^2\, 2\int_0^\infty \rho(p)\, dp = \left(\frac{d\sigma}{d\Omega_\gamma}\right)_{KN} \frac{K_0^2\langle p^{-2}\rangle}{2\pi} \tag{26}$$

where $\langle p^{-2}\rangle$ is a moment of the EMD (Epstein 1973, Wong *et al* 1975) and from (25)

$$d\sigma/d\Omega_\gamma = Z(d\sigma/d\Omega_\gamma)_{KN}. \tag{27}$$

The integrated counts of figure 4 (N_γ) and figure 5 (N_e) are proportional to the cross sections of (27) and (26), respectively. Thus, we obtain from the ratio of the total counts N_e/N_γ

$$\langle p^{-2}\rangle = (2\pi Z/K_0^2\, \Delta\Omega_e\, \varepsilon_e) N_e/N_\gamma \tag{28}$$

Here, $\Delta\Omega_e$ and ε_e are the solid angle and efficiency of the electron detector. By taking the ratio N_e/N_γ, trivial factors such as the Klein–Nishina cross section, solid angle and efficiency of the γ-detector, photon flux density etc have been eliminated. In deriving (26) we have assumed that the electron detector is placed at $p_\perp = 0$. With $Z = 29$, $K_0 = 62.1$ au, $\Delta\Omega_e = 0.3$ msr, $\varepsilon_e = 0.85$ and $N_e/N_\gamma = 0.027$ we arrive at $\langle p^{-2}\rangle = (5.0 \pm 1.4)$ au. The error results essentially from estimates of the uncertainties of the electron detector solid angle, its efficiency and the total counts N_e and N_γ. The experimental value shows fair agreement with the theoretical $\langle p^{-2}\rangle = 6.32$ au which we obtained from an integration of the MAPW density $\rho(p)$ (Bross 1982).

The evaluation of the differential cross sections for the electron branch follows from equation (23) and is similar to that of the photon branch. Since we have, from (10*b*),

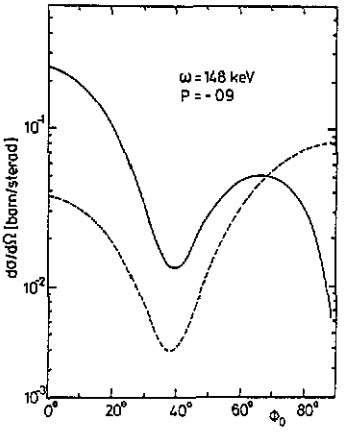

Figure 9. The single-differential cross section for the electron branch (solid curve) and the photon branch (broken curve) as a function of the electron emission angle φ_0.

$d\Omega_\gamma = dp_x\, dp_y/\kappa_0^2$—here, dp_x and dp_y are perpendicular to $\boldsymbol{\kappa}_0$ and differ from those of (24)—one obtains equivalently to (25)

$$\frac{d^2\sigma}{dE'\, d\Omega_e} = \left(\frac{d\sigma}{d\Omega_\gamma}\right)_{KN} \frac{\omega p_0'}{\kappa_0^3} J(p_z) = \left(\frac{d\sigma}{d\Omega_e}\right)_{KN} \frac{(1+\omega)}{(1+E_0')} \frac{1}{\kappa_0} J(p_z) \tag{29}$$

with p_z' of (10*a*). Notice, that the Klein–Nishina cross section now refers to the electron solid angle $d\Omega_e$. One further integration of (29) yields, together with (10*a*),

$$d\sigma/d\Omega_e = Z(d\sigma/d\Omega_e)_{KN}. \tag{30}$$

A quantity easily accessible by experiment is the ratio of the total single counts N_e/N_γ which determines the cross section ratio:

$$R \equiv (d\sigma/d\Omega_e)_{KN}/(d\sigma/d\Omega_\gamma)_{KN} = (\Delta\Omega_\gamma\, \varepsilon_\gamma/\Delta\Omega_e\, \varepsilon_e)N_e/N_\gamma. \tag{31}$$

From (2) one finds, for this ratio, (Davisson and Evans 1952, Heitler 1954)

$$R = |d\Omega_\gamma/d\Omega_e| = 4a^2 \cos\varphi_0/(\cos^2\varphi_0 + a^2 \sin^2\varphi_0)^2 \tag{32}$$

with $a = 1 + \omega$. For $\omega = 148$ keV and $\varphi_0 = 15.8°$ one has $R = 5.8$. For 80 nm and 290 nm thin Cu foils we have measured the count ratio $N_e/N_\gamma = 5.2$ and 6.0, respectively. With $\Delta\Omega_\gamma = 0.4$ msr and a γ-detector efficiency $\varepsilon_\gamma = 0.7$ the experimental cross section ratios are $R_{exp} = 5.7 \pm 1$ for the thinner foil and $R_{exp} = 6.5 \pm 0.4$ for the thicker one. The rather large error in the former case results from a background subtraction which amounted to about 90% of the total electron signal. As an illustration, we show in figure 9 the single-differential cross sections for the photon branch $(d\sigma/d\Omega_\gamma)_{KN}$ (broken curve) and the electron branch $(d\sigma/d\Omega_e)_{KN}$ (full curve). The curves hold for $\omega = 148$ keV and a linear polarization of the incident photon beam of 90% (i.e. a Stokes parameter $P = -0.9$ (Rollason *et al* 1989b, Smend *et al* 1987)). The agreement of the numbers above demonstrates that, on the one hand we understand the detection efficiency of our system, i.e. solid angles $\Delta\Omega$ and quantum efficiency ε, reasonably well and, on the other hand, that no electrons are lost or gained by scattering. We have investigated this point

more quantitatively. In analogy to (12) an effective single-differential cross section is calculated that is influenced by multiple scattering:

$$\langle\sigma(\varphi_0)\rangle_{\text{eff}} = P_0\sigma(\varphi_0) + 2(1 - P_0)\int_0^{\pi}\int_0^{\infty}\sigma(\varphi)g(p_\perp)p_\perp \,\mathrm{d}p_\perp \,\mathrm{d}\gamma \qquad (33)$$

with the abbreviation $\sigma = (\mathrm{d}\sigma/\mathrm{d}\Omega_e)_{\text{KN}}$ and

$$\varphi = [\varphi_0^2 + (\Delta\varphi)^2 - 2\varphi_0\Delta\varphi\cos\gamma]^{1/2}$$

where $\Delta\varphi = p_\perp/K_0$. With the multiple-scattering function $g(p_\perp)$ for the 80 nm Cu foil we find that the effective cross section is only 4% smaller than the undisturbed $\sigma(\varphi_0)$. This is a rather small difference especially in view of the 40% change in $\sigma(\varphi_0)$ within $\langle\Delta\varphi_0^2\rangle^{1/2} = \pm 3°$ which is approximately the angular width of the $g(p_\perp)$ distribution. Inspecting the angular behaviour of $\sigma(\varphi_0)$ in figure 9 we see that apparently as many electrons are scattered towards $\varphi_0 = 15.8°$ from smaller angles as are scattered away from φ_0 towards larger angles, thus compensating to first order the influence of multiple scattering.

6. Conclusions

The experiment has demonstrated that EMDs can, at least in principle, be extracted from a $(\gamma, e\gamma)$ experiment. Although the photon flux density has been increased considerably compared with that of our last experiment (Bell *et al* 1990) and is now at 2×10^{10} photons $\text{cm}^{-2}\,\text{s}^{-1}$, the data that have been accumulated in 33 hours of beam time still suffer from rather bad statistics. This can be overcome by several experimental efforts: the introduction of two-dimensional detectors, both γ- and/or electron detectors, the use of an insertion device like a wavelength shifter or an undulator, and the possibility of running the storage ring in a multi-bunch mode which would reduce the proportion of false coincidences. It might even be legitimate to dream of machines with rather large critical energies such as LEP or PETRA. The inevitable use of very thin solid state targets does not limit the evaluation of three-dimensional EMDs since monocrystalline metal foils are easily produced by epitaxy.

Acknowledgment

The authors are grateful to Th Kracht of HASYLAB, Hamburg, who developed the software for the data acquisition system.

References

Antonov A N, Hodgson P E and Petkov I Zh 1988 *Nucleon Momentum and Density Distributions in Nuclei* (Oxford: Clarendon)

Bell F, Rollason A J, Schneider J R and Drube W 1990 *Phys. Rev.* B **41** 4887–90

Berggren K-F *Phys. Rev.* B **6** 2156–61

Berko S 1983 *Positron Solid-State Physics, Proc. Int. Enrico Fermi School Physics, Course LXXXII* ed W Brandt and A Dupasquier (New York: North-Holland)

Bothe W and Geiger H 1925 *Z. Phys.* **32** 639–63

Bothe W and Maier-Leibnitz H 1936 *Z. Phys.* **102** 143–55

Bross H 1982 *J. Phys. F: Met. Phys.* **12** 2249–66
Brown D B, Wittry D B and Kyser D F 1969 *J. Appl. Phys.* **40** 1627–36
Byron F W Jr and Joachain C J 1989 *Phys. Rep.* **179** 211–72
Cashwell E D and Everett C J 1959 *The Monte-Carlo Method for Random Walk Problems* (New York: Pergamon)
Clementi E and Roetti C 1974 *At. Data Nucl. Data Tables* **14** 177–478
Cooper M J 1985 *Rep. Prog. Phys.* **48** 415–81
Cross W G and Ramsey N F 1950 *Phys. Rev.* **80** 929–36
Davisson C M and Evans R D 1952 *Rev. Mod. Phys.* **24** 79–107
Day D 1989 *Momentum Distributions* ed R N Silver and P E Sokol (New York: Plenum) pp 319
Epstein I R 1973 *Phys. Rev.* A **8** 160–8
Felsteiner J, Pattison P and Cooper M 1974 *Phil. Mag.* **30** 537–48
Fuggle J C and Martensson N 1980 *J. Electron Spectrosc. Relat. Phenom.* **21** 275–81
Gao C, Ritter A L, Dennison J R and Holzwarth N A 1988 *Phys. Rev.* B **37** 3914–23
Hansen N K, Pattison P and Schneider J R 1987 *Z. Phys.* B **66** 305–15
Hayes P, Bennett M A, Flexman J and Williams J F 1988 *Phys. Rev.* B **38** 13371–76
Hayes P, Williams J F and Flexman J 1991 *Phys. Rev.* B **43** 1928–39
Heitler W 1954 *The Quantum Theory of Radiation* 3rd edn (Oxford: Clarendon) p 220
Jauch J M and Rohrlich F 1955 *Theory of Photons and Electrons* (Cambridge, MA: Addison-Wesley)
Kwei C M 1984 *Thin Solid Films* **111** 83–92
Lencinas S, Burgdörfer J, Kemmler J, Heil O, Kroneberger K, Keller N, Rothard H and Groeneveld K O 1990 *Phys. Rev.* A **41** 1435–43
Manninen S, Hämäläinen K, Schneider J R and Rollason A J 1990 *Acta Crystallogr.* A **46** C-28
McCarthy I E and Weigold E 1988 *Rep. Prog. Phys.* **51** 299–392
Motz J W, Olsen H and Koch H W 1964 *Rev. Mod. Phys.* **36** 881–928
Paakkari T, Manninen S and Berggren K F 1975 *Phys. Fenn.* **10** 207–12
Pages L, Bertel E, Joffre H and Sklavenitis L 1972 *At. Data* **4** 1–69
Pattison P, Hansen N K and Schneider J R 1982 *Z. Phys.* B **46** 285–94
Persiantseva N M, Krasilnikova N A and Neudachin V G 1979 *Zh. Eksp. Teor. Fiz.* **76** 1047–57 (Engl. Transl. 1979 *Sov. Phys.-JETP* **49** 530–35)
Platzman P M and Tzoar N 1965 *Phys. Rev.* A **139** 410–3
Reimer L 1984 *Transmission Electron Microscopy (Springer Series in Optical Sciences 36)* (Berlin: Springer)
Ritter A L, Dennison J R and Jones R 1984 *Phys. Rev. Lett.* **53** 2054–7
Rollason A J, Bell F and Schneider J R 1989a *Nucl. Instrum. Methods* A **281** 147–55
Rollason A J, Bell F, Schneider J R and Drube W 1989b *Solid State Commun.* **72** 297–300
Rubinstein R Y 1981 *Simulation and the Monte Carlo Method* (New York: Wiley)
Salvat F 1991 *Phys. Rev.* A **43** 578–81
Salvat F, Martinez J D, Mayol R and Parellada J 1986 *Comput. Phys. Commun.* **42** 93–104
Salvat F and Parellada J 1984a *J. Phys. D: Appl. Phys.* **17** 185–201
—— 1984b *J. Phys. D: Appl. Phys.* **17** 1545–61
Smend F, Schaupp D, Czerwinski H, Schumacher M, Millhouse A H and Kissel L 1987 *Phys. Rev.* A **36** 5189–99
Wong T C, Lee J S, Wellenstein H F and Bonham R A 1975 *Phys. Rev.* A **12** 1846–58